Re-entry event prediction through the analysis of optical sensor data gathered from a worldwide network of telescopes

Krzysztof Kamiński, Justyna Gołębiewska, Monika K. Kamińska, Edwin Wnuk
Astronomical Observatory Institute, Faculty of Physics, A. Mickiewicz University, Poznan
Michał Żołnowski, Marcin Gędek
6ROADS Sp. z o. o., Krakow

Marek Polewski
Faculty of Power and Aeronautical Engineering, Warsaw University of Technology

Abstract

The article presents two methods for predicting the re-entry of an object into the atmosphere. The first method utilizes astrometric results from optical observations of objects in low Earth orbits (LEO) collected over the two months preceding the predicted re-entry time. These observations were carried out using a global network of telescopes belonging to the Astronomical Observatory of Adam Mickiewicz University (AMU) and the company 6ROADS. These data allow for refining the orbit, atmospheric drag parameters and ballistic coefficient, significantly increasing the accuracy of determining the final re-entry time. The second described method is based on the analysis of historical data from the USSPACECOM TLE catalog and orbital data in TLE format obtained from the optical observations. Matching the propagation results with the updated TLE catalog, enriched with new observations, enables the precise determination of the ballistic coefficient, which in turn allows for more accurate re-entry predictions.

1. INTRODUCTION

Observed in recent years, increasing deployment of satellites in the Earth's orbits is leading to a vast increase in the number of artificial objects in the Earth's vicinity. This makes the task of maintaining situational awareness and space traffic management an increasing challenge in the life cycle of these objects. This concerns the management of these objects' end-of-life phase. The foundation for effective implementation of this activity is awareness and the ability to accurately predict the behavior of an object just before and during its atmospheric re-entry. As such, it is possible to carry out the process of removing decommissioned objects in a planned manner without endangering any active ones in the vicinity and minimizing the likelihood of hazardous materials reaching the Earth's surface. For uncontrolled atmospheric re-entry, the ability to accurately predict the trajectory and impact location is essential to implement timely evacuation measures and emergency response protocols, protecting both human life and property. Consequently, monitoring of satellite re-entry becomes an essential element to ensure the overall safety and well-being of the civilian population.

Despite these challenges, results from sample observations and improved orbits demonstrate that difficulties associated with passive optical observations of LEO objects approaching re-entry can be overcome. This paper presents the results of observations, orbit improvements, re-entry moment predictions, and a comparison with predicted re-entry moments based on the analysis of historical Two-Line Element (TLE) data and other re-entry services, which are publicly available.

The improvement of accuracy in predicting re-entry moments and determining the geographical locations of satellite objects falling to Earth is becoming a crucial and urgent issue. This is due to the substantial increase in the number of objects being deployed in Earth's orbits, especially those with large dimensions and high mass. Contemporary methods for enhancing orbits and predicting re-entry moments primarily rely on radar observations conducted in the period preceding re-entry, often spanning 30 or 60 days before the given satellite object's re-entry.

LEO orbits are heavily influenced by the Earth's atmosphere, hence all orbit determination and trajectory prediction calculations of objects moving to re-entry have to be performed applying the effects of the atmospheric drag with very high accuracy. Apart from orbital parameters, the object's drag coefficient C_d and the ballistic coefficient BC also have to be estimated.

In the context of refining these processes, optical observations executed using a global network of wide-field telescopes seem to be a significant tool. Such observations can effectively contribute to enhancing the orbits of objects approaching re-entry.

2. TELESCOPE NETWORK

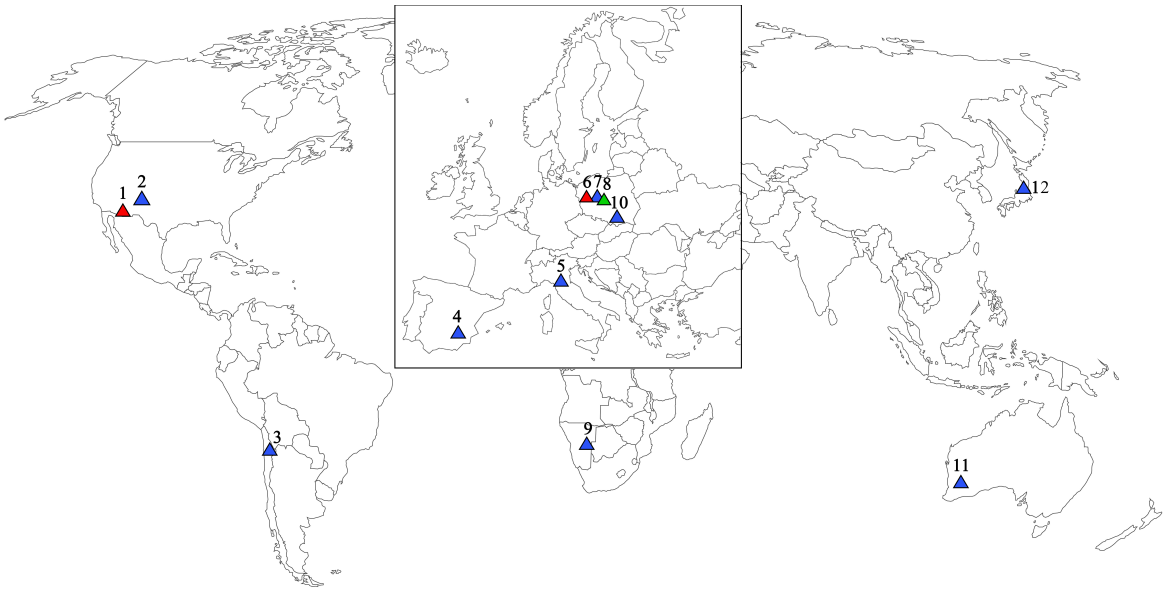

Figure 1: AMU (red) and 6ROADS (blue) observatories. 1 - PST2, 2 - Beata, 3 - Polonia, Polonia II, 4 - Idgrasil A, Idgrasil B, 5 - Rantiga, Rantiga 2S, Rantiga 2N, 6 - PST3 A, B, C, D, E, 7 - Oborniki, Wojnówko, 8 - Borowiec, 9 - Moonbase, 10 - Solaris, 11 - Marta, 12 - Anjin-San.

Test observations carried out with AMU PST3e telescope in June 2023 confirmed the effectiveness of optical observations of pre-reentry satellites. Systematic observations covered approximately 10 objects approaching re-entry over a period of several days, preceding the re-entry moment by 2-4 weeks. The application of a global telescope network significantly increases the likelihood of visibility and the potential number of optical observations of a given LEO object in the period preceding re-entry. Therefore, an experiment was conducted to demonstrate the usefulness of a global optical sensor network (Fig. 1).

The optical observations of LEO objects were made in collaboration between the Astronomical Observatory of the Adam Mickiewicz University (AMU) and the 6ROADS company using telescopes located all over the globe (Europe, Africa, North and South America, Asia, Australia). AMU was using its PST3e telescope, which is a 0.3m f/1.0 Sonnefeld optical system instrument with Andor Zyla sCMOS camera in its prime focus. The field of view (FoV) is 2.4 x 3.2 deg and pixel scale 4.5 arcsec/pix. The telescope uses a fast direct-drive Planewave L-500 mount, GNSS receiver for accurate image timing and a custom, in-house developed, automatic observation and reduction software (PSST - Poznań Satellite Software Tools).

6ROADS is a privately owned entity with 14 optical telescopes located in eleven locations on six continents. The main activity of the company focuses on optical observations of Resident Space Objects in frames of Space Traffic Management and Planetary Defence. 6ROADS telescopes have fields of view from 0.18 to 6.47 square degrees, with the average value for the whole network of 2.29 square degrees. For the purpose of this campaign, we used seven telescopes on five continents. All of them are RASA (Rowe-Ackermann Schmidt Astrograph) optical design. Five of

them have 11" and two of them 14" primary mirrors. Relatively fast optics (f/2.2) combined with high QE (up to 90%) sCMOS sensors delivers a setup capable of efficient observation of satellites on LEO orbits. The majority of telescopes is operated with direct drive mounts, allowing precise tracking of fast moving objects. Rantiga observatory was the only location where survey instead of tracking was applied. Traditional gear-type mount did not allow for precise tracking and thanks to relatively large FoV efficient survey was possible. In this campaign, we used observatories with two kinds of setups. Observatories Beata, Oborniki, Polonia II, Rantiga 2S and Anjin-San have relatively small FoV - 0.68 square degrees and yield pixel scale of 0.97 arcsec/pixel. Observatories Rantiga and Moonbase have much larger FoV - 4.59 square degrees with similar pixel scale of 0.98 arcsec/pixel.

The approach to data reduction in the 6ROADS network depends on local speed of Internet. In our case, this last mile problem determines if obtained data may be reduced on central servers in Poland or must remain on local computers. In case of LEO satellites, usually large amount of data is generated during a single pass over the observatory. This approach is to secure the number of frames with sufficient number of reference stars to perform accurate astrometry. Two types of sCMOS yielded two types of data. Camera QHYCCD 174 GPS generates only 4.4 MB per single frame, while the second sensor, QHYCCD 600 Pro, delivers 29.4 MB per frame, which requires high computing power to deliver reduced data in timely manner. It is important to stress out, that QHYCCD 600 Pro has a rolling shutter leading to characteristic image skewing of fast moving objects. Such distortion caused by non-simultaneous readout was corrected in the post-processing, before data reduction.

3. OBSERVATION CAPABILITIES OF THE RE-ENTRY EVENT THROUGH OPTICAL TELESCOPE NETWORKS

Observations of an object just prior to its re-entry event with an optical telescope are inherently difficult. Most of these objects are on very low Earth orbits at altitudes of the order of 300 km a few weeks before re-entry. This translates to high angular velocities, which for circular orbits are observed between about 2 deg/s at zenith and 0.15 deg/s at the altitude of 15 deg above horizon. Because of that the effective exposure time is also very short - between 0.0003 and 0.004 seconds respectively. By effective we mean that longer exposure time will result in trailed images of stars (in satellite tracking observations) or trailed images of satellites (in sidereal tracking observations). The result is a severely reduced limiting magnitude of the not tracked objects, which for a 0.3m telescope is of the order of 12 mag. Obviously, a large field of view is preferred, not only to increase the number of reference stars in satellite tracking observations, but also to offset the inaccuracies of ephemeris. On the other hand, low orbiting satellites have increased observed brightness when compared to more distant targets. At the altitude of 300 km, a spherical diffusing satellite with the diameter of 1m and albedo of 0.2 has observed brightness of approximately 7 mag at zenith and from 9 mag to 12 mag at 15 deg (depending on phase angle).

The observing windows for objects on such low orbits from a single location are also very short. In the most advantageous situation of a satellite pass at 300 km altitude, assuming that we can observe it from 15 deg above horizon through zenith down to 15 deg, it can last about 4 min. Of course such situation is rare. Already at the solar altitude of about 9 deg below horizon it becomes possible that a satellite at 300 km orbit will be hidden in the Earth's shadow when located 15 deg above the horizon. With the Sun below -25 deg all such objects will be passing in the sky always hidden in the Earth's shadow. This gives a very short observing window of typically 1.5 to 3 h per night, depending on observer's latitude and season. Any possible unfavourable weather conditions at the observing site will also add up to the limitations. Therefore, a network of relatively small, large FoV, tracking optical instruments is preferred to increase the effectiveness of monitoring satellites prior to their re-entry.

Astrometric observations obtained from such a network allow to improve the orbit and other parameters of a given object, in particular the parameters related to modeling the influence of the Earth's atmosphere on the motion of an object close to re-entry. Further propagation of the orbit from these determined and corrected parameters and the determination of the re-entry moment become much more accurate, and the uncertainties of the re-entry moment and predicted location decrease significantly.

Using software developed at AMU, an analysis was carried out for several objects approaching re-entry in July and August 2024 of their potential visibility from the telescope network described in the previous section. Table 1 contains numbers of visible passes of each object from each observatory in the network. The following assumptions were made: the object is not hidden in the shadow of the Earth - it is illuminated by the Sun, the Sun is at least 12 degrees below the horizon, the object passes >15 degrees above the horizon. The visibility analysis spanned from July 1-14, 2024.

Observatory	Object - NORAD Cat. Number						
	14819	49067	43690	49789	45788	55887	39369
Borowiec, Poland	17	6	0	4	5	0	0
Chalin, Poland	17	5	0	3	4	0	0
Winer, Arizona	0	0	8	2	6	0	3
Idgrasil, Spain	0	8	10	7	8	0	0
Oborniki, Poland	17	6	0	3	5	0	0
Rantiga, Italy	8	17	7	11	12	0	0
Solaris, Poland	18	10	2	6	9	0	0
Wojnowko, Poland	17	6	0	3	5	0	0
Anjin-San, Japan	0	4	9	5	7	0	3
Polonia, Chile	0	0	0	0	0	21	1
Beata, Rowe, USA	0	0	8	4	7	0	5
Moonbase, Namibia	0	0	0	0	0	22	0
Marta, Australia	0	0	0	0	0	27	0

Table 1: Number of visible passes for all observatories.

Observatory	Object - NORAD 12155	
	1.07 - 14.07.2024	15.07 – 31.07.2024
Borowiec, Poland	0	6
Chalin, Poland	0	7
Winer, Arizona	0	6
Idgrasil, Spain	0	8
Oborniki, Poland	0	6
Rantiga, Italy	0	10
Solaris, Poland	0	7
Wojnowko, Poland	0	6
Anjin-San, Japan	0	8
Polonia, Chile	4	4
Beata, Rowe, USA	0	8
Moonbase, Namibia	4	3
Marta, Australia	5	2

Table 2: Number of visible passes of object 12155 for all observatories.

The results presented in Table 1 clearly show very different conditions of visibility of selected objects for individual observatories. The time intervals in which passes are visible are very short - up to a few minutes, sometimes even only 2-3 minutes. At the same time, it turns out that the numbers of visible passes are generally large enough to effectively observe such objects, but these observations must be precisely planned and carefully executed.

Observations of objects approaching re-entry should be carried out sufficient time in advance. Some objects are unavailable for observations from almost all telescopes of the network for weeks, while within the following weeks the number of observable passes may be appropriate. An example is the NORAD 12155 object, which re-entry took place on August 23, 2024. In the Table 2 the numbers of visible passes of 12155 are presented for two intervals: July 1-14, 2024 and July 15-31, 2024. The differences in numbers of visible passes from different observatories are significant.

4. OBSERVATIONS

The presented analysis of the impact of optical observations on the determination of expected re-entry moment was mostly performed based on optical astrometric observations of selected objects approaching re-entry, carried out in June and July of 2024. An additional data set collected in 2023 with PST3 telescopes for object numbered 52323 has

NORAD	Observatory	Date
49789	RANTIGA IIB	04.07.2024
	PST3	05.07.2024
	RANTIGA IIB	05.07.2024
	RANTIGA IIB	10.07.2024
14819	PST3	28.06.2024
	PST3	29.06.2024
	PST3	04.07.2024
	PST3	05.07.2024
	PST3	09.07.2024
55067	BEATA	29.06.2024
12155	RANTIGA	30.07.2024
52323	PST3	01.06.2023
	PST3	03.06.2023
	PST3	04.06.2023
	PST3	05.06.2023
	PST3	06.06.2023
	PST3	07.06.2023
	PST3	11.06.2023

Table 3: Data series for objects approaching re-entry selected for analysis in this work.

been included in the analysis.

Table 3 contains the full list of data sets used for the orbital analysis: orbit determination and correction and orbit propagation until the time of re-entry.

5. ORBIT DETERMINATION

5.1 Software description

In this study, Orbit Determination (OD) and re-entry prediction of LEO objects were performed with a software tool based on Orekit package. Orekit is a free, open source, low-level space dynamics library written in Java that aims at providing accurate and efficient components for the development of flight dynamics applications. It is designed to be easily used in very different contexts, from quick studies up to critical operations. Orekit Software is developed inside CS Group and distributed under the Apache License version 2.0 [2].

The entire program used for calculations is described in Figure 2. There are two parts, orbit determination and re-entry prediction, that can be run independently and can take calculation results from one another. This functionality allows for enhanced and independent orbit determination.

5.2 Orbit determination and orbit propagation specification

LEO orbits are heavily influenced not only by the Earth's gravity field, but by atmospheric drag as well. Hence all orbit determination and orbit propagation calculations have to take into account the best avaiable atmospheric model and geopotential model with harmonic coefficients up to a very high degree and order. Apart from orbit parameters, the object's drag coefficient C_d and ballistic coefficient BC has to be estimated.

In all calculations the applied force model includes:

- Earth's gravity field: 70x70 with EGM-2008 model,
- third bodies: Sun and Moon with JPL ephemeris,
- atmospheric drag with NRLMSISE-00 model with space weather parameters from AGI website [1],
- solar radiation pressure.

The propagator was specified to use the DormandPrince853 integrator with minimal step 0.001s, maximum 300s and position error set to 10^{-4}m. For both OD and re-entry prediction the same propagator and the same force model was used.

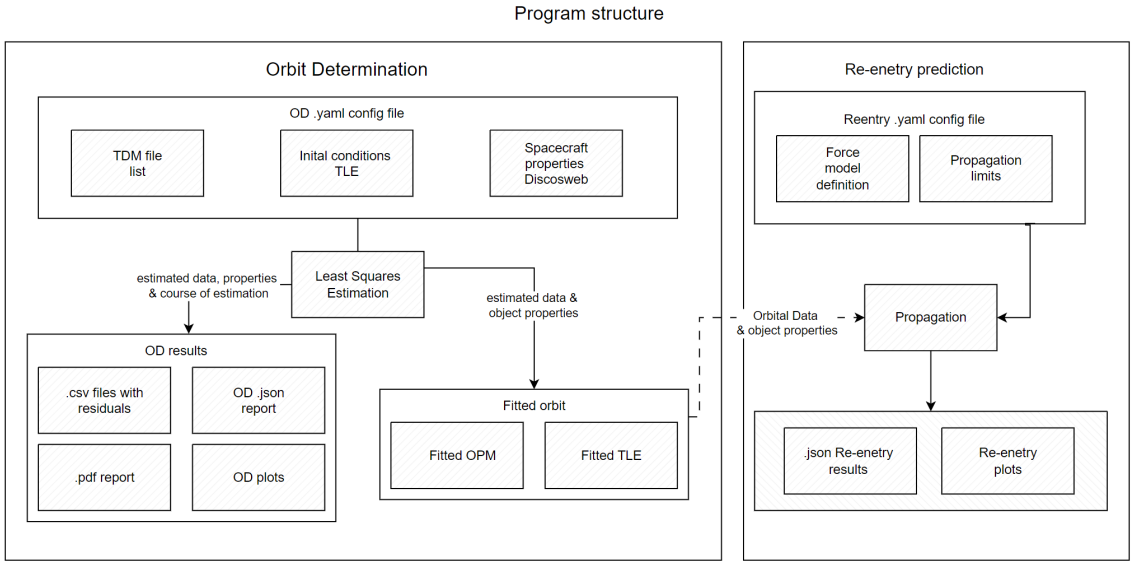

Figure 2: Data flow chart in orbit determination and re-entry prediction calculations.

The estimator's settings were often adjusted, because some of them did not yield convergent solutions for all objects. Some of the calculations converged after 15 iterations, other after even 30 iterations.

The following specification of the estimator was applied:

- convergence criterion: $\varepsilon = 10^{-3}$,
- weight: 1 (all observations had the same weight),
- faulty observation rejection after 6 consecutive iterations.

Before each OD calculation it was necessary to specify the mass, area and initial drag coefficient of an object. Mean cross-section and mass values were taken from the Discos database maintained by Space Debris Office at ESA. It is worth noting that not all objects in Discos have physical properties assigned.

5.3 Orbit determination workflow

As visible in Figure 2, observational data are provided in the Tracking Data Message (TDM) format in accordance with the CCSDS standard for Tracking Data Message version 2. Fetched measurements included time, right ascension (RA), declination (Dec) and brightness.

During calculations, each satellite followed the same process, which included the following steps:

- Execution of single OD using Space-Track [3] Two Line Elements (TLE) as initial orbit parameters for the first batch of observation files and generation of a new, fitted TLE and an Orbit Parameter Message (OPM).
- Execution of single OD using previously generated TLE as an initial condition for another batch of observation files, and again, generation of a fitted TLE and OPM.

Due to the nature of LEO orbit estimation, it was often necessary to rerun the program with modifications in the configuration file. In some cases (especially in the case of object 49789, for which there are no physical properties listed in Discos database) it was also necessary to guess the mass, mean cross-section and initial value of C_d. This fact posed a major challenge, as even small changes in the initial value of any parameter led to noticeably different rates of convergence. Also, diverging processes were common.

5.4 Orbit determination results

Example results of OD for objects from Table 3 are presented in this section. Fitted orbits were mostly successfully calculated from 2-3 consecutive passes. Estimated parameters included not only orbital parameters, but also the drag

coefficient C_d. Then the orbit propagation for re-entry prediction can be obtained with good results. In case of one pass, OD was also possible with sufficient quality, however re-entry prediction was not achievable with good accuracy due to issues with C_d estimation.

Object 14819 - batch 1

OD initial conditions:

- TLE epoch: 24180.80280743
- Mass $m = 1982$ [kg]
- Mean cross section $A = 13.217\ m^2$
- $C_d = 2.0$

OD results:

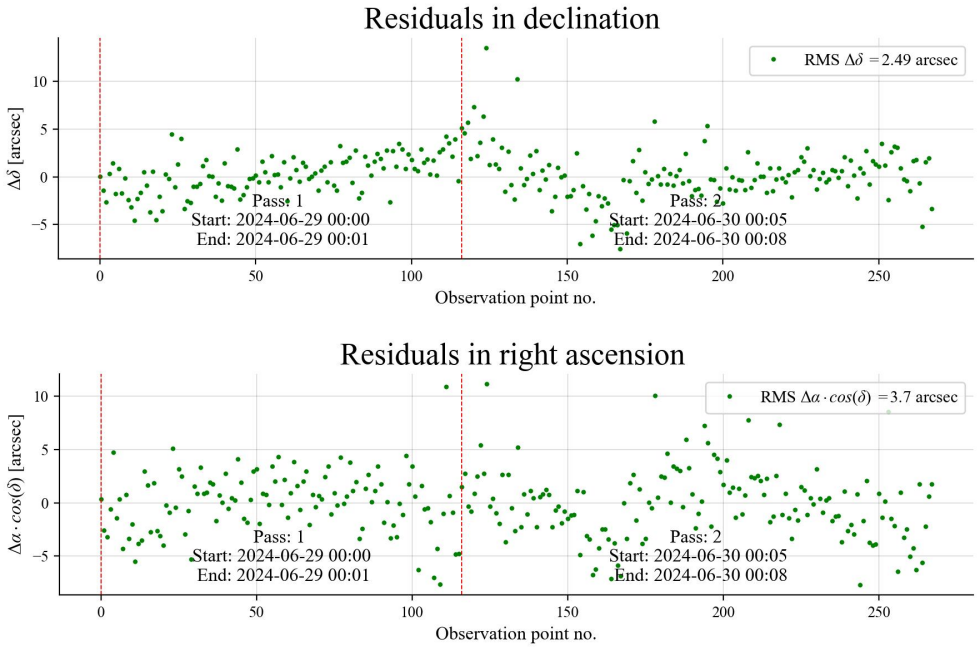

Figure 3: Residuals in right ascension and declination for object 14819.

Number of observation points: 268
Epoch of estimated elements: 2024-06-28 19:16
Estimated $C_d = 2.18$
Estiamted TLE:

```
1 14819U 84027A   24180.80280743  .00414812  65945-4  11400-2 0  9992
2 14819  82.4599 294.1698 0009134 259.6987 100.3629 15.93811933209469
```

Object 14819 - batch 2

OD initial conditions:

- TLE epoch: 24186.82150658
- Mass 1982 $[kg]$
- Mean cross section $A = 13.217\ m^2$
- $C_d = 2.0$

OD results:

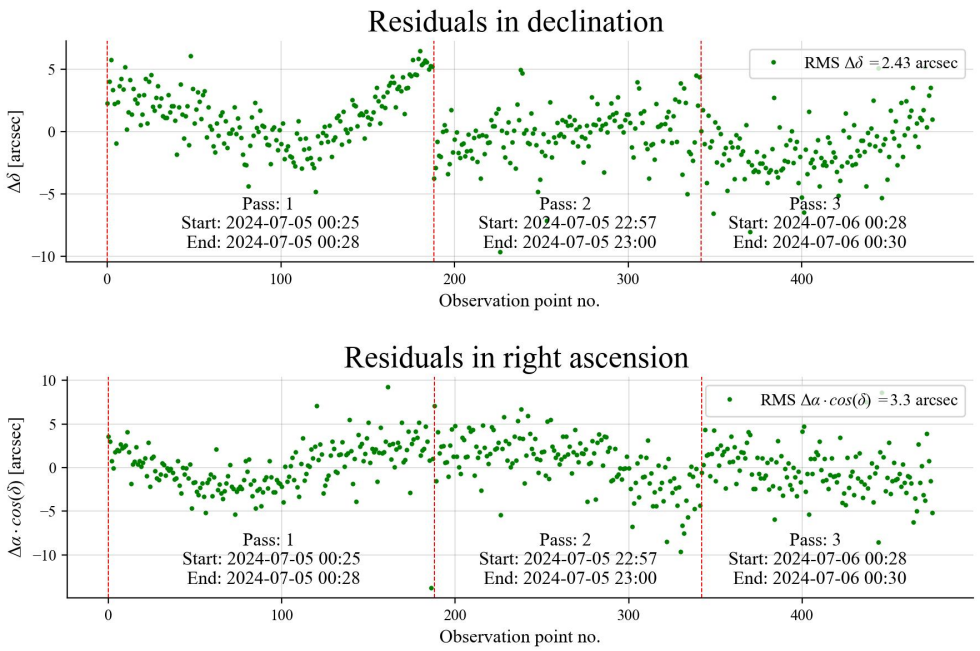

Figure 4: Residuals in right ascension and declination for object 14819.

Number of obervation points: 476
Epoch of estimated elements: 2024-07-04 19:42
Estimated $C_d = 2.08$
Estimated TLE:

```
1 14819U 84027A   24186.82150658  .00405608  66908-4  87164-3 0  9995
2 14819  82.4600 287.4284 0009439 247.2688 112.7503 15.98408601210163
```

Object 49789

OD initial conditions:

- TLE epoch: 24186.587
- Mass 100.0 $[kg]$
- Mean cross section $A = 1.414\ m^2$
- $C_d = 2.0$

OD results:

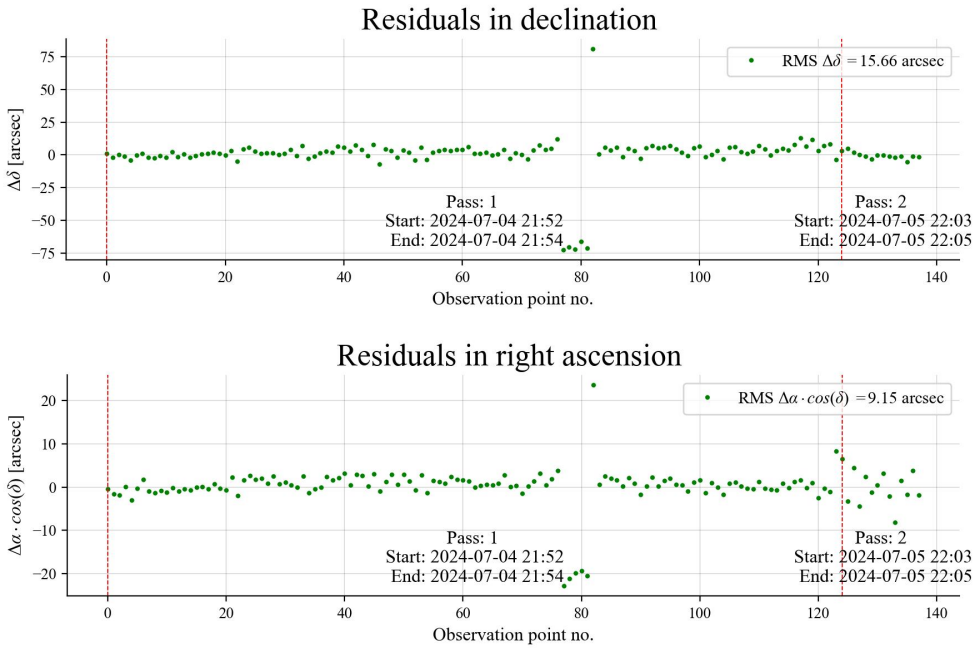

Figure 5: Residuals in right ascension and declination for object 49789.

NUmber of observation points: 138
Epoch of estimated elements: 2024-07-04 14:05
Estimated $C_d = 2.80$
Estimated TLE:

```
1 49789U 82092JF  24186.58736631  .00474403  80741-4  17543-2 0  9996
2 49789  82.5867 253.0544 0029331 245.7301 114.0479 15.87446430146119
```

Object 52323 - batch 1

OD initial conditions:

- TLE epoch: 23152.95002953
- Mass 4000 $[kg]$
- Mean cross section $A = 23.715\ m^2$
- $C_d = 2.0$

OD results:

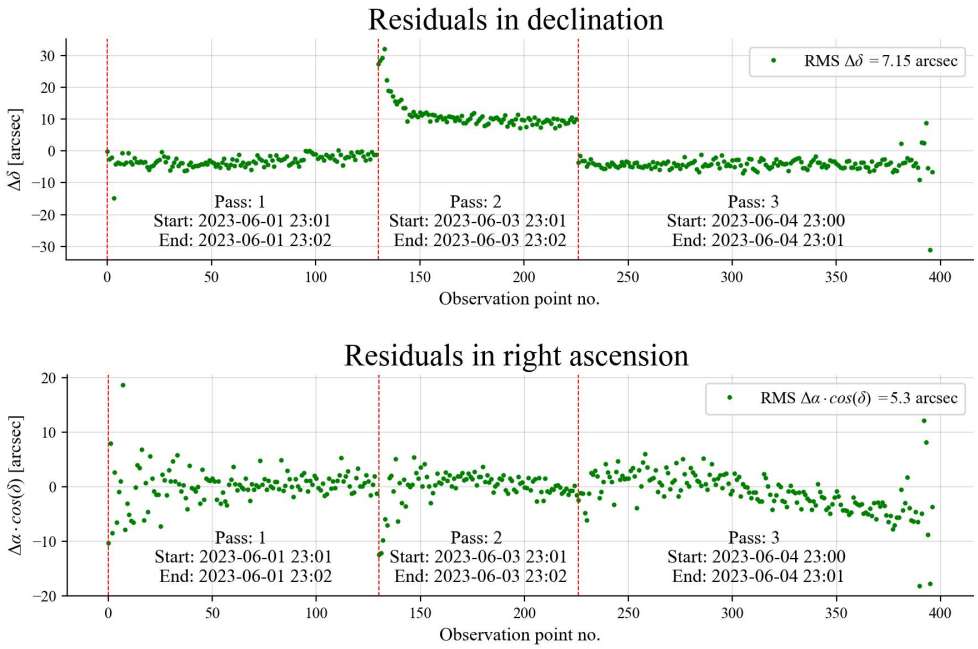

Figure 6: Residuals in right ascension and declination for object 52323.

Number of observation points: 397
Epoch of estimated elements: 2023-06-02 19:48
Estimated $C_d = 2.40$
Estimated TLE:

```
1 52323U 22043D   23152.95002953  .00460713  94016-4  87507-3 0  9997
2 52323  97.5470 257.7369 0002075 349.1096  11.2288 16.00122939 62085
```

5.5 Problems encountered during OD calculation

Throughout the entire calculation campaign, multiple challenges were encountered.

- The best results were achieved when the epoch of initial conditions (especially from SpaceTrack) was in the middle of observations sequence (eg. TDM from 10.06 to 14.06, initial condition from 12.06).
- In some cases, for the first estimation, it was necessary to use more accurate data than TLE.
- In some cases initial guesses of C_d was making estimation divergent.
- Many estimations failed, it was necessary to readjust the estimator settings.

6. ANALYSIS AND RESULTS OF SATELLITE RE-ENTRY PREDICTIONS

6.1 Re-entry prediction with the use of optical observations

Predicted re-entry epochs for three exemplary objects listed in section 5.4 were determined using numerical integration propagator and taking into account estimated orbital and atmospheric drag parameters as initial conditions. Two independent sets of re-entry prediction calculations were conducted: first with initial condition including estimated in OD process orbital elements and drag coefficient C_d and the second one with the original values of USSPACECOM TLE elements and estimated C_d parameter.

Predicted re-entry epochs obtained from the first set of calculations are presented in Table 4. Table 5 presents results of both sets of calculation in comparison with the re-entry epochs obtained by using the method based on historical TLE elements. Re-entry window in Table 4 is defined as 0.20 of time span between the epoch of estimated orbit and predicted re-entry epoch. The same definition is applied by Space-Track. Results presented in Table 4, for all analyzed objects, show very good agreement between decay epoch from Space-Track and the re-entry epoch obtained from calculations based on astrometric observations from optical telescopes. One has to note that the epoch of estimated orbital elements obtained from telescope observations is much earlier than the MSG epoch in the Space-Track data and values of re-entry widows are very different. Optical astrometric observations seem to be very useful in the re-entry service.

Norad	**Days of observations**	**Epoch of estimated orbit**	**Re-entry epoch from OD**	**Re-entry window from OD (min)**	**Re-entry epoch from Space-Track**		
					MSG epoch	**Decay epoch**	**Window (min)**
14819	2024 June 29 - 30	28.06.2024 19:16	23.07.2024 17:16	7000	19.07.2024 18:44	23.07.2024 22:58	1140
	2024 July 5-6	04.07.2024 19:42	23.07.2024 03:21	5450	20.07.2024 22:30	23.07.2024 22:58	900
	Final reentry epoch from Space-Track: 23-07-2024 20:33						
49789	2024 July 4-5	04.07.2024 14:05	20.07.2024 00:05	3860	17.07.2024 20:36	20.07.2024 00:00	-
	Final reentry epoch from Space-Track: 20-07-2024 00:00						
52323	2023 June 1-3	01.06.2023 22:48	20.06.2023 08:57	5800	16.06.2023 09:29	20.06.2023 07:59	1140
	2023 June 4-6	02.06.2023 19:48	20.06.2023 07:48	5300	-	-	-
	2023 June 7-11	02.06.2023 19:48	20.06.2023 10:32	5340	-	-	-
	Final re-entry epoch from Space-Track: 20-06-2023 18:04						

Table 4: Re-entry predictions for objects 14819, 49789 and 52323.

Predicted re-entry epochs obtained by the second set of calculations with the use of original USSPACECOM TLE and estimated value of C_d presented in Table 5 are very close to that obtained from the first set of calculations. This means that proper determination of the C_d parameter in the OD process with the use of optical observations is crucial for re-entry prediction with high accuracy.

6.2 Method based on historical orbital elements

As demonstrated in the publication [5], prediction of the decay epoch of an object orbiting in the Earth's atmosphere strongly depends on accurate values of the ballistic coefficient (BC) used in the calculations of the object's predicted trajectory and on the Earth's atmospheric density calculated from an applied atmospheric model with the current space weather data. Therefore, the most crucial aspect of this method is the precise estimation of the BC value.

In this study, BC values were obtained using the method described in [5] by fitting the calculated predicted trajectory to the trajectory described by the TLE Catalog orbital data. Example fitting results for the object 49789 are presented in figure 7. The fitting method is based on the differential correction applied to historical TLE data. The catalog orbital data for given epochs are taken as "observations" O (marked in red in the figure 7), and orbital elements calculated for these epochs with the use of the STOP orbit predictor are taken as "calculated values" C (marked in blue in the figure 7). Differential correction process adjusts the value by minimizing the residuals. The USSPACECOM TLE historical

data for a given satellite object, sourced from the Satellite Catalog (space-track.org), were supplemented with orbital elements determined from observations conducted by our telescope network, as described in the previous chapter of this work.

The general concept of the method used is relatively straightforward: the decay epoch for a given object (the time at which the object will reach a specific altitude above the Earth's ellipsoid, e.g., 90 km) is determined by orbital prediction starting from a specific epoch, with initial conditions derived from TLE orbital elements at this epoch and the ballistic coefficient value obtained through a fitting process utilizing all TLE data from the initial epoch to the epoch before the expected decay epoch. The final elements (green dot in Figure 7) in the used TLE catalog were determined from observations conducted by our telescope network, as described in this study.

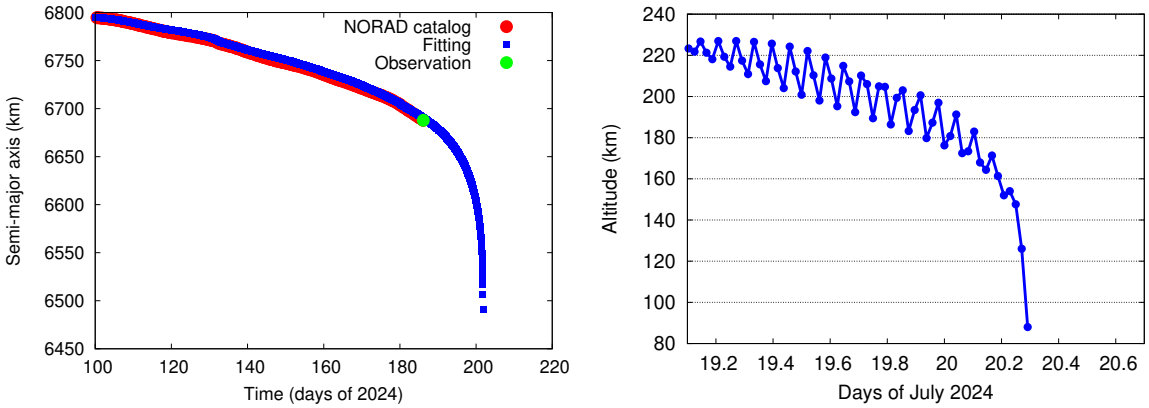

Figure 7: Predicted semi-major axis and altitude evolution before re-entry for object 49789.

The propagation of orbits in this method was performed using STOP – The Short-Term Orbit Propagator – a software tool developed at the Astronomical Observatory of Adam Mickiewicz University [6]. The numerical version of STOP (which employs numerical integration of the equations of motion) was used with the following force model: geopotential zonal and tesseral harmonic coefficients up to the 30th degree and order, luni-solar effects, solar radiation pressure with cannonball modeling, and inclusion of Earth's shadow effects, atmospheric drag using the NRLMSISE-00 model of the atmosphere and historical values of the geomagnetic planetary index and solar flux. These data were acquired from the CelesTrak website (https://celestrak.org). Initial conditions for the numerical integration were obtained by transforming mean TLE orbital elements at the epoch into osculating orbital elements using the algorithm presented in [4].

Norad	**Re-entry from TLE propagation BC**	**Re-entry from TLE propagation with estimated C_d**	**Re-entry epoch from OD**	**Re-entry epoch from Space-Track**
14819	23.07.2024 14:20	23.07.2024 04:21	23.07.2024 17:16	23.07.2024 22:58
		23.07.2024 14:42	23.07.2024 03:21	23.07.2024 22:58
49789	20.07.2024 07:00	20.07.2024 01:05	20.07.2024 00:05	20.07.2024 00:00
52323	20.06.2023 23:40	20.06.2023 11:07	20.06.2023 08:57	20.06.2023 07:59
	-	-	20.06.2023 07:48	-
	-	-	20.06.2023 10:32	-

Table 5: Comparison of results from different re-entry prediction methods.

As a result of the aforementioned propagation, the predicted evolution of the semi-major axis and altitude leading up to re-entry was obtained. The evolution of altitude for object 49789, 24 hours prior to re-entry, is presented in Figure 7b. The estimated time of re-entry is July 20th at 7:00 AM. Based on the described procedure, the moment of re-entry for objects 14189 and 52323 were also determined. Historical data from the USSPACECOM catalog were supplemented with orbit determination results in the TLE format, presented in section 5.4. The resulting set of elements was used to

fit the optimal values of the ballistic coefficient BC through numerical integration of the equations of motion. Using the BC values obtained in this way, the re-entry times were determined and listed in Table 5 in the "Re-entry from TLE propagation BC" column.

7. CONCLUSIONS

Optical observations of very low LEO objects approaching re-entry pose a challenge, requiring the application of special strategies and consideration of difficulties associated with high velocities of these objects.

Ephemeridal calculations for several objects approaching re-entry for the Polish telescope network indicate that most objects generate enough observable passes. However, some of these passes are relatively short in duration and occur low above the horizon. Therefore, they require short exposure times during observations and special astrometric processing of images.

Using a global network of wide-field telescopes it is possible to collect sufficient number of astrometric observations that allow accurate orbit determination of LEO objects 30 - 60 days before re-entry.

Optical telescope observations seem to be a significant tool in re-entry service. Such observations can effectively contribute to enhancing the orbits of objects approaching re-entry.

Predicted re-entry epochs obtained with the use of two methods presented in this paper are very close to the decay epoch given by Space-Track.

8. REFERENCES

[1] Cssispaceweather. [Online].: `https://ftp.agi.com/pub/DynamicEarthData/SpaceWeather-v1.2.txt`.

[2] orekit.org. [Online].: `https://www.orekit.org`.

[3] Space-track.org. [Online].: `https://www.space-track.org`.

[4] Wnuk E. Recent progress in analytical orbit theories. *Advances in Space Research*, 23:677–687, 1999.

[5] Mikołaj Krużyński, Zygmunt Anioł, Krzysztof Armiński, Dorota Mieczkowska, Marcin Teofilewicz, Edwin Wnuk, Zubowicz Tomasz, Justyna Gołębiewska, Monika K. Kamińska, Krzysztof Kamiński, Dorota Krużyńska, Julia Pietrzak, and Marek Poleski. Influence of the atmosphere model and the quality of the ballistic coefficient (BC) estimation on the prediction of the re-entry moment. In S. Ryan, editor, *The Advanced Maui Optical and Space Surveillance Technologies Conference*, page id128, September 2023.

[6] Edwin Wnuk. STOP - The Short-Term Orbit Propagator. In *Kepassa2015, 28-30 October 2015 Toulouse*, 2015.